



**HAL**  
open science

## Towards an improved rapid assessment tool for rockfall protection forests using field-mapped deposited rocks

Julia Menk, Frédéric Berger, Christine Moos, Luuk Dorren

### ► To cite this version:

Julia Menk, Frédéric Berger, Christine Moos, Luuk Dorren. Towards an improved rapid assessment tool for rockfall protection forests using field-mapped deposited rocks. *Geomorphology*, 2023, 422, pp.108520. 10.1016/j.geomorph.2022.108520 . hal-04021032

**HAL Id: hal-04021032**

**<https://hal.inrae.fr/hal-04021032>**

Submitted on 9 Mar 2023

**HAL** is a multi-disciplinary open access archive for the deposit and dissemination of scientific research documents, whether they are published or not. The documents may come from teaching and research institutions in France or abroad, or from public or private research centers.

L'archive ouverte pluridisciplinaire **HAL**, est destinée au dépôt et à la diffusion de documents scientifiques de niveau recherche, publiés ou non, émanant des établissements d'enseignement et de recherche français ou étrangers, des laboratoires publics ou privés.



Distributed under a Creative Commons Attribution - NonCommercial - NoDerivatives 4.0 International License



# Towards an improved rapid assessment tool for rockfall protection forests using field-mapped deposited rocks

Julia Menk<sup>a</sup>, Frédéric Berger<sup>b</sup>, Christine Moos<sup>a</sup>, Luuk Dorren<sup>a,\*</sup>

<sup>a</sup> Bern University of Applied Sciences BFH-HAFL, Laenggasse 85, Zollikofen 3052, Switzerland

<sup>b</sup> French National Institute for Agriculture, Food, and Environment INRAE, 2 rue de la Papeterie, Saint Martin d'Heres 38402, France

## ARTICLE INFO

### Keywords:

Energy line  
Rockfall  
Protection forest  
RockFor<sup>NET</sup>  
Rockfall model

## ABSTRACT

In steep, mountainous terrain, protection forests play a key role in rockfall risk prevention, because trees reduce the energy of falling blocks or even stop them. The simple but robust tool RockFor<sup>NET</sup> (RFN) models the protective effect of forests in order to assess the residual rockfall hazard. It uses the energy line principle with a fixed energy line angle (ELA) to derive the rockfall energy that has to be dissipated by the forest. The objective of this study was firstly to empirically reconstruct the ELA and initial fall heights of field-mapped rockfall deposits on 16 forested slopes in Switzerland. The second objective was to assess to what extent RFN can be improved by estimating trajectory-specific ELAs as well as better representative initial fall height values for rock faces. The analysis showed that the prediction of the protective capacity of a forest could substantially be improved by using transect-specific ELAs and more specific initial fall height values, especially for block volumes between 0.2 and 1 m<sup>3</sup>. Furthermore, we found a strong relationship between the retro-calculated ELAs and the normalized area below the rockfall trajectories, indicating that the normalized area is a promising method for deriving trajectory specific ELAs.

## 1. Introduction

Rockfall is a natural hazard which occurs spontaneously in relief-rich areas all over the world and can cause damage to settlements and infrastructure or even loss of lives (Heinimann et al., 1998; Borella et al., 2019). It is extremely difficult to ensure constant and countrywide protection against such a widely dispersed natural hazard, which is also very difficult to predict in its temporal occurrence and maximum intensity. Currently, protection against rockfall generally focuses on the prevention of its occurrence, e.g., rock clearance and blasting, and on the reduction of its impact, e.g. with structural measures like nets and dams, or biological ones like forests.

Forests play an important role in rockfall risk prevention, because trees act as individual barriers that reduce the kinetic energy of falling blocks or even stop them (Dorren et al., 2007; Dorren and Wehrli, 2013). On slopes where the protective effect of forests does not suffice to reduce rockfall risks to an acceptable level, costly engineered structures, such as flexible rockfall nets, are needed. Also there, the engineered measures are often more cost-effective (lower installation and/or maintenance costs) due to the protective effect of the forest. Therefore, protection forests play often a key role in the integrated natural-hazard risk

management strategies of mountainous countries, amongst others the one of Switzerland (Dorren and Wehrli, 2013). On average, protection forests can reduce rockfall occurrence by up to 90 % and rockfall intensity by up to 70 %, if the essential factors such as forested slope length, tree density, tree diameter, horizontal forest structure, and rock volume are appropriate (Moos et al., 2017). Recently, different modelling approaches have been developed to quantify the protective effect of trees against rockfall, ranging from empirical models in 2D (e.g., Berger and Dorren, 2007) to more complex processed-based models simulating rebounds on single trees in 3D (e.g., Dorren, 2016; Lu et al., 2021).

Since forest structure, in combination with the forested slope length, is one of the important variables governing the level of protection against rockfall (Frehner et al., 2007; Dorren et al., 2015), it is in many cases necessary to manage the forests in order to optimize its protective function in the long term (Wehrli et al., 2006). Switzerland has therefore developed the NaiS management guidelines (“sustainability and success monitoring in protection forests”) (Frehner et al., 2005), which define principles of silvicultural decision-making and provide target values for protection forests (e.g., stem number per hectare, gap size, crown cover) to ensure their sustainable management (Frehner et al., 2007).

The core of the NaiS rockfall protection guidelines is a simple but

\* Corresponding author.

E-mail address: [luuk.dorren@bfh.ch](mailto:luuk.dorren@bfh.ch) (L. Dorren).

<https://doi.org/10.1016/j.geomorph.2022.108520>

Received 1 April 2022; Received in revised form 4 November 2022; Accepted 5 November 2022

Available online 26 November 2022

0169-555X/© 2022 The Author(s). Published by Elsevier B.V. This is an open access article under the CC BY-NC-ND license (<http://creativecommons.org/licenses/by-nc-nd/4.0/>).

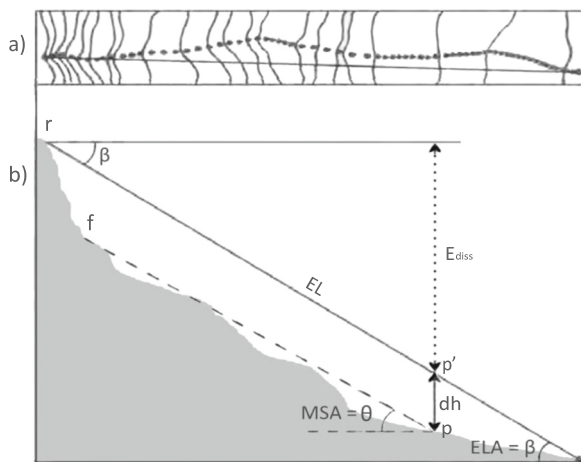


**Fig. 1.** The energy line principle explained with (a) the top view of a rockfall trajectory and (b) its profile view. EL: energy line between the rock release point *r* and the terrain intersection point; ELA ( $\beta$ ): energy line angle; MSA ( $\theta$ ): mean slope angle;  $E_{diss}$ : dissipated energy;  $dh$ : energy head. Adapted from Berger and Dorren (2007).

**Table 1**  
Compilation of studies applying the energy line principle with different ELAs (sorted ascending by ELA).

Source	ELA value(s)
Wieczorek et al. (1999)	22°–30°
Berger and Dorren (2007)	27°–34°
Corominas et al. (2003)	27°–55°
Onofri and Candian (1979)	28°–42°
Scheidegger (1973)	29°–40°
Meissl (1998)	29°–49°
Dorren et al. (2005)	31°–38°
Hsü (1975)	32°
Žabota et al. (2019)	32°
Jaboyedoff and Labiouse (2011)	32°–36°
Jaboyedoff and Labiouse (2003)	33°
Heinimann et al. (1998)	33°–37°
Toppe (1987)	33°

robust and user-friendly tool called RockFor<sup>NET</sup> (RFN) (cf. [www.rockfor.net](http://www.rockfor.net)). It is an empirically-based approach used to model and quantify the protective effect of forested areas in 2D (Berger and Dorren, 2007). The tool also provides the theoretically required stand density and the number of stems per diameter class required for optimal protection. This characteristic defines the target profile of a given protection forest. The latter is derived from the kinetic energy of the rockfall that has to be dissipated by the forest. To calculate this energy, the current version of RFN makes use of the energy line principle (see further information in Section 2) with a fixed energy line angle (ELA) of 31°, regardless of the local topography. Based on the same principle, RFN also indicatively estimates the protective capacity of a forest against rockfall. Although RFN has been used for more than ten years, both by practitioners and in several scientific studies (e.g., Maringer et al., 2016; Saroglou et al., 2015; Borgniet et al., 2013), its scientific validity has only been tested by Berger and Dorren (2007).

Our hypothesis is that the predictions of the protective capacity provided by RFN can be improved by accounting for variations in the topography along rockfall trajectories in the definition of the used ELA. A preliminary empirical study of well-documented historical rockfall events presented a method that allows for taking such variations into account when estimating the ELA of a given rockfall trajectory profile (cf. Quarteroni, 2017).

RFN requires the initial fall height (FH) of a released block from a given rock face, which, however, varies over time since rock do not fall

from the same location all the time. Moreover, the impact energy of a rock falling down a 200 m rock face is not necessarily equal to its kinetic energy after a 200 m vertical drop, as energy is dissipated during rebounds on rock edges in the rock face. As a result, it is challenging to define an appropriate value for the initial fall height, as required by RFN. Currently, RFN uses a logarithmic function to translate the total height of the rock face into an energetically representative initial fall height to prevent too pessimistic protection estimations. However, this approach has only been validated with a very limited number of well-documented rockfall events so far.

Hence, the question arises to what extent a site adapted ELA instead of a fixed angle of 31° and an accurately estimated initial fall height improves the evaluation of the protective capacity of a rockfall forest. To answer this question, we empirically reconstructed the ELA and initial fall heights of field-mapped rockfall deposits on 16 forested slopes in Switzerland. We then evaluated the accuracy of RFN by quantifying the protective effect of the forest covering the studied sites and assessed to what extent RFN can be improved by estimating more accurate trajectory-specific ELAs and initial FHs.

## 2. Theoretical background

### 2.1. The Energy Line Principle

The *Energy Line Principle* was first described by Heim (1932), who showed that the total travel distance of a falling rock can be described by an imaginary energy line (EL) which connects the rockfall release zone with the stopping point of the fallen block (Fig. 1).

The EL indicates at any point *p* along the rockfall trajectory how much kinetic energy has been dissipated (see  $E_{diss}$  in Fig. 1) and how much potential energy remains that can be transformed into kinetic energy ( $E_{kin}$ ) (Erismann and Abele, 2001; Hantz et al., 2021). This remaining energy can be calculated as

$$E_{kin} = E_{pot} = m \cdot g \cdot \delta h \quad (1)$$

where *m* is the mass of the rock (in kg), *g* is the acceleration due to gravity (9.81 m·s<sup>-2</sup>) and  $\delta h$  is the height difference between the energy line at point *p'* and the terrain at point *p* (from now on referred to as *energy head*). When  $\delta h$  equals zero, all the kinetic energy has been dissipated and the block stops moving (Berger and Dorren, 2007; Wyllie, 2014).

Although the energy line principle is only a very general approach to assess rockfall runout zones, it is often used for preliminary hazard assessment, both in practice and in research. In the current literature, a range of different ELAs with a median value of 29° (Table 1) is used.

### 2.2. Principles of RockFor<sup>Net</sup> (RFN)

RFN applies the energy line principle to quantify the kinetic energy that needs to be dissipated by a forest in the rockfall transit area. As described by Berger and Dorren (2007) and Dorren et al. (2015) it transforms the existing forest into a given number of virtual barriers (determined by the stem density of the forest) consisting of trees standing in a horizontal line. These barriers can dissipate a given amount of energy (determined by the mean diameter at breast height (DBH) and the tree species in the forest). The protective capacity of the forest is finally expressed as the percentage of blocks stopped by the forest at a given point *p* along a forested slope (Fig. 1).

RFN requires only a few input parameters to characterize the terrain, i.e., the total height of the rock face, the length of the forested and non-forested slope below the rock face, and the mean slope angle. The modelled falling block is described by its three dimensions (height, width and depth in m), its shape (rectangular or ellipsoid) and its density (in kg·m<sup>-3</sup>). The forest is represented by the stem density (ha<sup>-1</sup>) and the mean DBH or the basal area (BA) of trees with a DBH ≥ 8 cm (BA he total

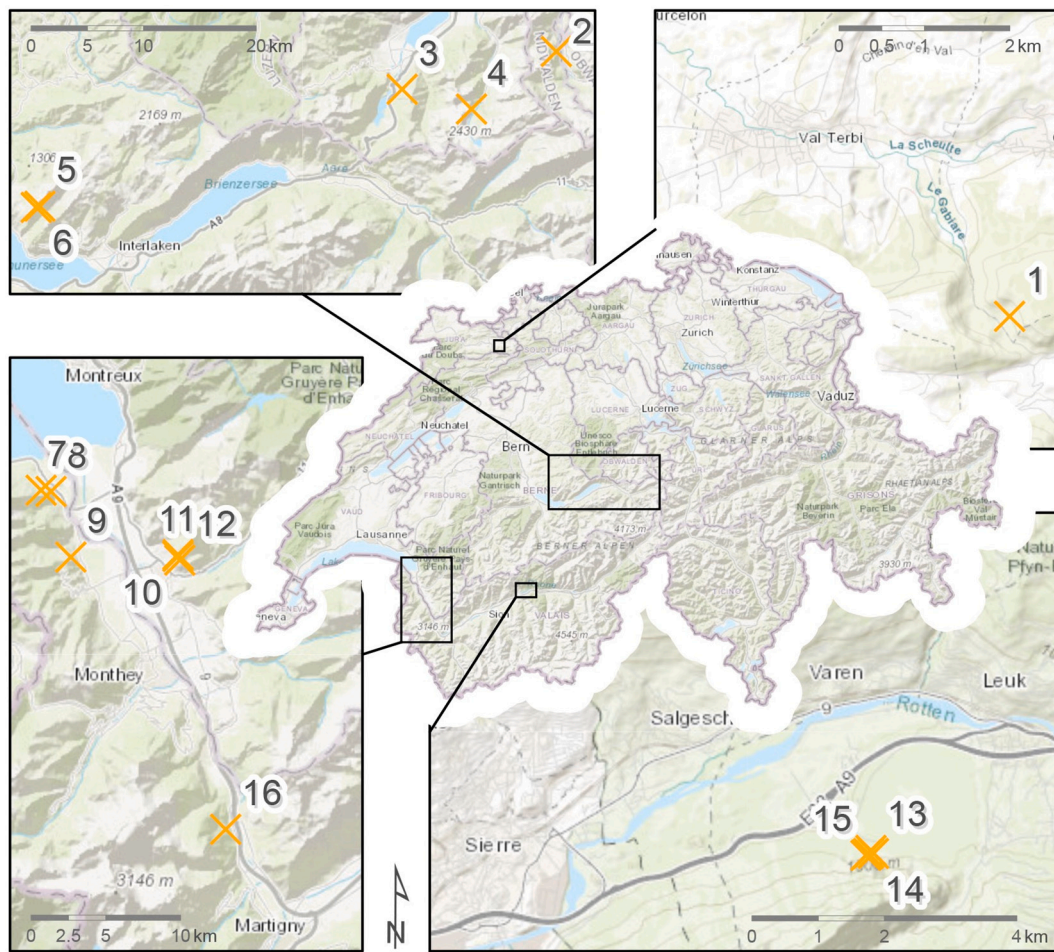


Fig. 2. Study area with the locations of the 16 rockfall trajectory transects (background: ESRI basemap).

Table 2

Summary of the data inventoried on the 16 transects. Start elev. = the elevation of the upper point of the transit slope. Vert. dist. = the vertical distance between the foot of the rock face and the last deposited block. Forest slope (plan.) = the planimetric length of the forested part of the slope. Conf. = the average proportion of coniferous trees on the transect.

Transect	Start coordinates [EPSG:21781]	Start elev.[m]	Vert. dist. [m]	Nr. transect sectors	Rock face height [m]	Slope angle (Std.) [°]	Forest slope [m]	Mean stem number [ha <sup>-1</sup> ]	Mean basal area [m <sup>2</sup> ha <sup>-1</sup> ]	Conf.
1	600780/242220	600	91	16	30	32.4 (2.1)	135	474	39.2	40
2	670620/188360	920	241	40	300	36.3 (2.0)	322	957	44.6	33
3	656940/184990	1050	272	41	200	40.1 (4.5)	319	921	70.6	19
4	663060/183270	1420	158	22	450	34.8 (0.6)	179	1158	50.8	77
5	624750/174620	1600	266	43	35	36.4 (1.0)	339	725	52.5	87
6	624430/174500	1715	276	38	40	43.9 (3.7)	267	689	56.2	97
7	555240/135370	885	220	33	100	39.7 (3.7)	234	892	37.1	34
8	555920/135260	610	220	30	30	38.0 (1.2)	234	1076	33.0	0
9	557230/130920	640	237	37	50	40.8 (2.2)	264	780	34.0	0
10	564400/130950	865	246	41	18	37.2 (1.8)	333	782	43.8	18
11	564400/131050	900	284	45	35	38.5 (1.5)	360	814	43.8	6
12	564510/130700	865	236	36	60	38.3 (2.1)	280	859	38.8	3
13	613450/127020	730	63	13	200	26.3 (2.3)	114	588	20.3	64
14	613370/127010	740	101	17	200	32.4 (2.3)	142	754	27.7	74
15	613340/126980	765	98	12	300	35.3 (0.9)	98	520	20.1	78
16	567570/112690	715	203	29	45	41.0 (1.6)	196	714	53.4	51

cross-sectional area of all stems in a stand measured at breast height and usually expressed per ha), as well as the proportion of the dominant tree species (in %).

If the rock face is higher than 10 m, RFN translates this height ( $H_{tot}$ ) into an energetically representative initial fall height  $FH_{RFN}$  (in m) as follows:

$$FH_{RFN} = 6.2 \cdot \ln(H_{tot}) - 4.5 \tag{2}$$

$FH_{RFN}$  can be interpreted as an estimate of the average block release elevation in the considered rock face. Then, based on  $FH_{RFN}$  and a fixed ELA of 31°, RFN calculates the total rockfall energy that needs to be dissipated by the forest until a specific point of interest along the forested slope (e.g., at its down-slope limit). The fixed ELA corresponds

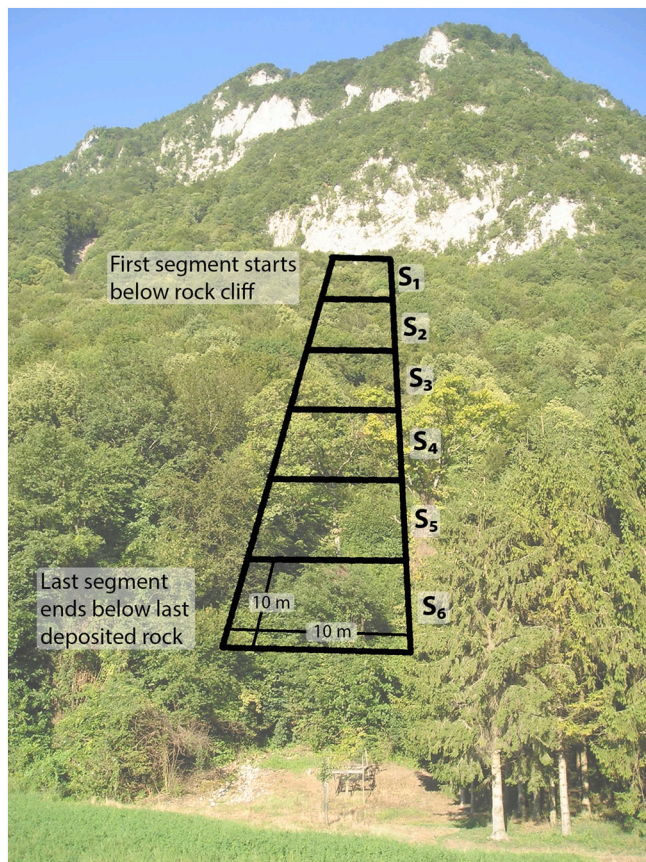


Fig. 3. Sketch of a typical rockfall transect divided into multiple sectors ( $S_1, S_2, \dots, S_n$ ) used for the field inventory.

Table 3  
Nr. of recorded blocks per transect (T) and rock volume class (RVC).

RVC	0.02	0.2	1.0	All
Volume [ $m^3$ ]	0.01–<0.02	0.02–<0.2	0.2–≤1.0	-
RVC diameter [m]	0.27	0.59	1.0	-
T	Number of recorded blocks			Sum
1	17	17	4	38
2	190	158	12	360
3	141	70	4	215
4	29	44	21	94
5	105	46	11	162
6	7	10	6	23
7	211	141	10	362
8	60	53	5	118
9	41	20	1	62
10	129	83	10	222
11	35	30	0	65
12	55	46	9	110
13	30	28	19	77
14	32	42	13	87
15	24	20	10	54
16	268	207	9	484
<b>Sum</b>	<b>1374</b>	<b>1015</b>	<b>144</b>	<b>2533</b>

to that observed during the real-size rockfall experiments on a non-forested slope of 38° described by Dorren et al. (2005). The results of these experiments were used to calibrate also the other parameters used in RFN.

Based on the total kinetic energy that has to be dissipated, RFN estimates the number of trees, or more precisely the basal area, required to stop all blocks at that specific point of interest, using the algorithms presented in Dorren and Berger (2006). Finally, RFN calculates the ratio

between the required and existing basal area in the given forest. This ratio corresponds to the percentage of rocks stopped by the forest. Changing conditions along the transect, such as the forest density, the basal area, the topography or soil roughness, have an influence on rock kinematics and the integration of these parameters would further increase prediction precision (Caviezel and Gerber, 2018; Vick et al., 2019). However, as they are highly variable and generally challenging and laborious to determine, they are not taken into account in RFN, because it would no longer fulfil its purpose as a rapid assessment tool for forests practitioners that allows assessing rockfall protection forests.

### 3. Materials

#### 3.1. Study sites

For this study, we inventoried 16 active forested rockfall sites throughout Switzerland (Fig. 2 and Table 2) with the following characteristics:

- transition and deposition areas were situated within the forested part of the slope;
- deposition areas were if possible undisturbed (i.e., absence of areas where rocks would be removed by humans);
- the steepness of the transit area was relatively linear (i.e., the slope angle was similar in the upper, central and lower parts);
- deposited block volumes were as diverse as possible;
- all other potential influences were as uniform as possible.

#### 3.2. Surveyed transects

At each survey site, we inventoried a sample area in the form of a long continuous strip (hereafter called transect) along the steepest down-slope descent below an active rockfall release area (see Fig. 3). Each transect started directly at the foot of the rock face and ended where no more freshly deposited rocks were found or at the lower limit of the forested slope. A transect was divided into sectors with a width and a surface length of 10 m (measured along the slope). Only in one case (transect 9) the transect terminated around 100 m before the lower limit of the forested slope due to the presence of a forest road crossing the transect. For every transect, we determined the total height of the rock face using a 1:25,000 topographical map with contour lines at an equidistance of 10 m (Swisstopo LK25; Swisstopo (2014)).

To extract the transect surface we used the DTM *swissALTI3D* (Swisstopo, 2014). This raster dataset has a spatial resolution of 2 × 2 m and is derived from aerial laser-scan data (LIDAR) and 3D stereo images recorded between 2002 and 2013 (positional accuracy of the laser points ± 0.5 m).

#### 3.3. Forest stands

Within each transect, we recorded the tree species as well as the DBH of all the trees with a DBH ≥ 8 cm and calculated the mean stem number and basal area per hectare. There were no continuous rockfall couloirs or large gaps along the transect. Obstacles other than standing trees (e.g., tree stumps, lying trunks, root plates, small trees, shrubs, surface roughness such as old rockfall deposits), which are important elements for energy loss along the rockfall trajectory as shown by many studies (e.g., Dorren et al., 2004; Bourrier et al., 2012; Lanfranconi et al., 2020; Lu et al., 2021), were not taken into account into the analysis performed in this study. This is because, at present, the effect of such obstacles cannot be taken into account in an energy line approach. At the same time, although not entirely similar, all slopes had sectors with quite some roughness in the form of the deposited rocks or in occasional cases also deposited tree stems, as well as sectors without obstacles other than standing trees.

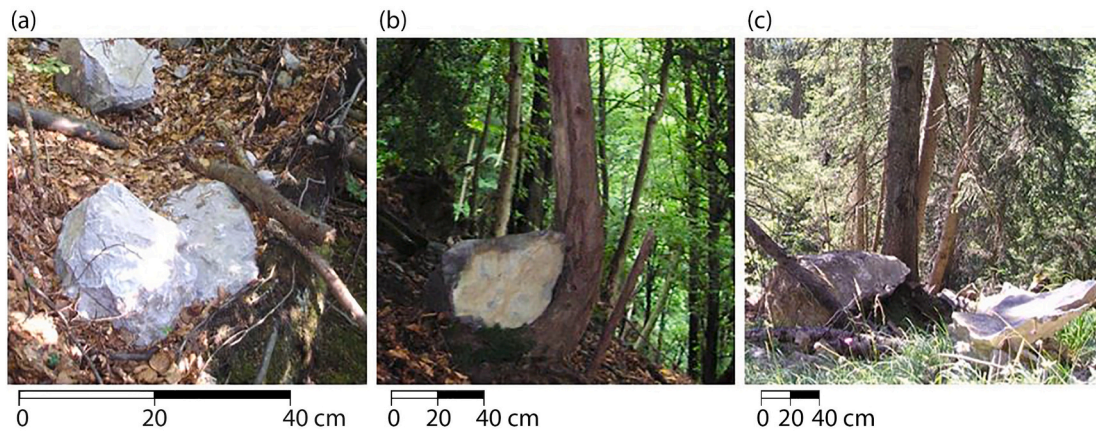


Fig. 4. Visualisation of the three RVCs; a block with (a) 0.02 m<sup>3</sup>, (b) 0.2 m<sup>3</sup>, and (c) 1 m<sup>3</sup>.

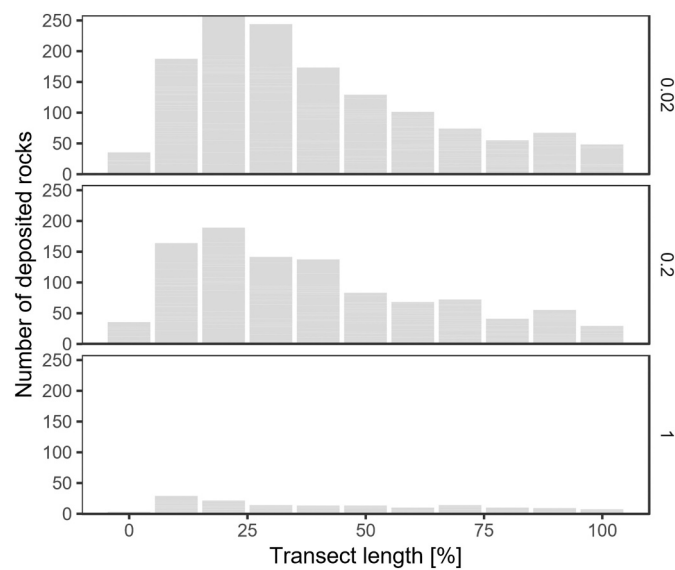


Fig. 5. Cumulative distribution of the deposited blocks along the transects for the three RVCs.

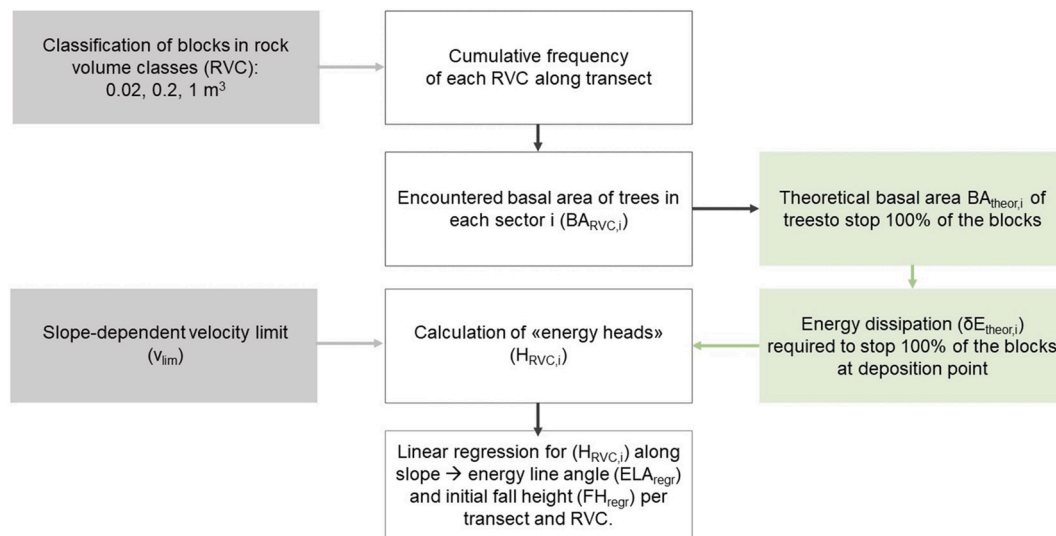
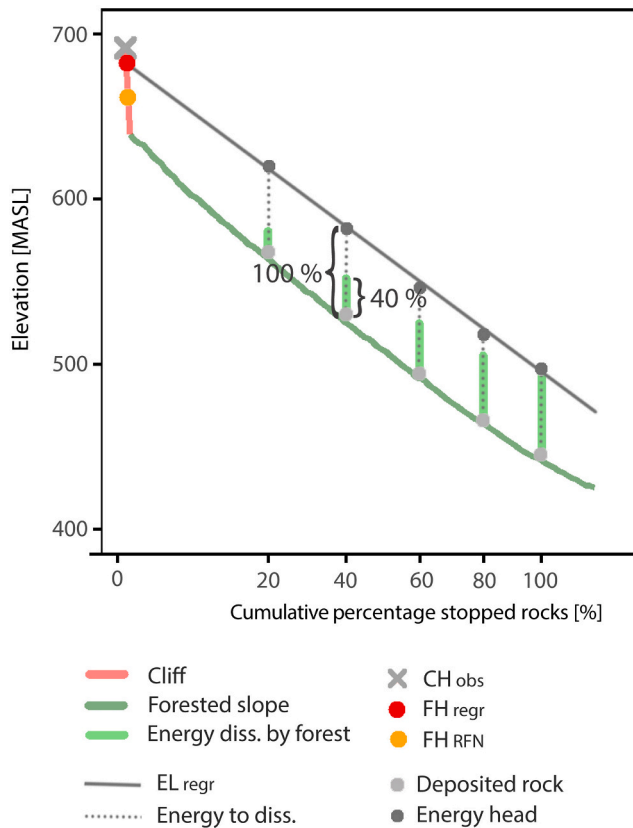


Fig. 6. Workflow of the methodology to derive slope and rock volume specific energy line angles (ELA) and initial fall heights (FH).



**Fig. 7.** Visualisation of the regression for determining the representative energy line for each transect and RVC.  $CH_{obs}$ : total rock face height observed in the field;  $FH_{RFN}$ : FH determined by RFN according to Dorren et al. (2015);  $EL_{regr}$ : energy line resulting from linear regression of the energy heads;  $FH_{regr}$ : intercept of the energy heads representing the fall height of that specific RVC and transect.

**Table 4**

$ELA_{regr}$  values per transect (T) and RVC. The column *all RVC* shows the results for all blocks combined per transect. Missing values are transects where no specific ELA could be calculated due to insufficient regression points. Potential outliers are indicated with \*.

T	RVC 0.02	RVC 0.2	RVC 1.0	All RVC
1	31.3	31.1	25.6*	30.4
2	34.7	34.9	34.2	34.3
3	38.2	37.5	34.1	37.3
4	35.0	33.5	37.0	34.9
5	35.3	35.3	33.3	35.0
6	40.3	39.3	36.1	38.9
7	37.6	37.3	33.1	36.8
8	37.4	37.2	36.0	36.8
9	36.8	38.4	–	37.5
10	35.8	35.8	33.7	35.6
11	37.2	36.9	–	37.0
12	37.5	37.5	37.9	37.5
13	25.4*	20.5*	24.4*	27.1
14	32.9	26.4	27.2*	29.5
15	33.8	30.2	33.5	31.4
16	40.2	40.2	44.5*	39.2

**3.4. Deposited blocks**

We inventoried all freshly or recently deposited blocks with a volume  $\geq 0.01 \text{ m}^3$  along each transect (i.e., no moss cover, non-weathered rock surface indicating fresh fragmentation, not firmly anchored in the ground). The maximum considered volume was  $1.0 \text{ m}^3$ , since we only found two blocks with larger volumes ( $1.3$  and  $1.5 \text{ m}^3$ , which were therefore not statistically representative). Old deposited blocks were not inventoried, as they were most probably not stopped by the current forest stand and were considered a potential bias for this study. The volume of the deposited rocks was calculated based on the measurement of the three main axes and an estimated correction factor (0.52 for a perfect sphere and 1 for a perfect cuboid). They were then classified into three rock volume classes (RVC):  $\geq 0.01$  and  $< 0.02 \text{ m}^3$  (referred to as RVC 0.02),  $\geq 0.02$  and  $< 0.2 \text{ m}^3$  (RVC 0.2) and  $\geq 0.2$  and  $< 1.0 \text{ m}^3$  (RVC 1.0) (Table 3 and Fig. 4).

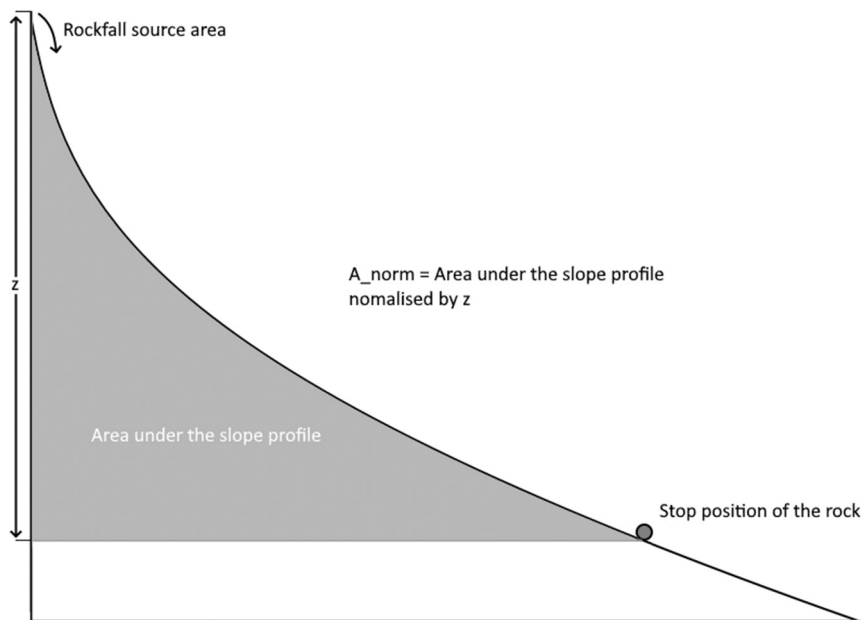


**Fig. 8.** Illustration of the normalized area below the slope profile of a given rockfall event.

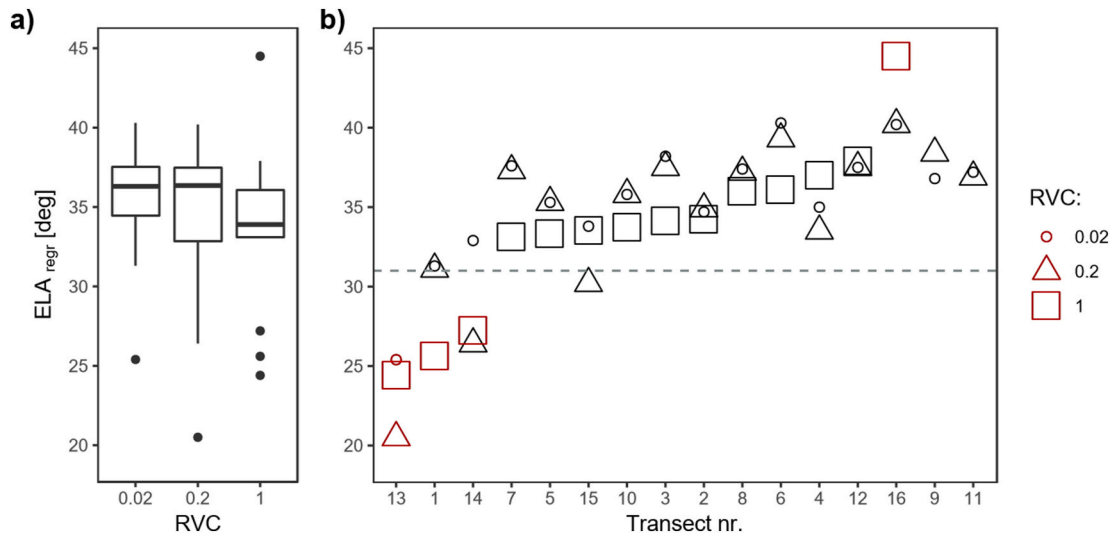


**Fig. 9.** (a) Distribution of the retro-calculated ELA (ELA<sub>regr</sub>) per RVC. (b) ELA<sub>regr</sub> per transect and RVC, sorted by the ELA of RVC 1.0 m<sup>3</sup>. Outliers based on the boxplot are indicated in red. (For interpretation of the references to color in this figure legend, the reader is referred to the web version of this article.)

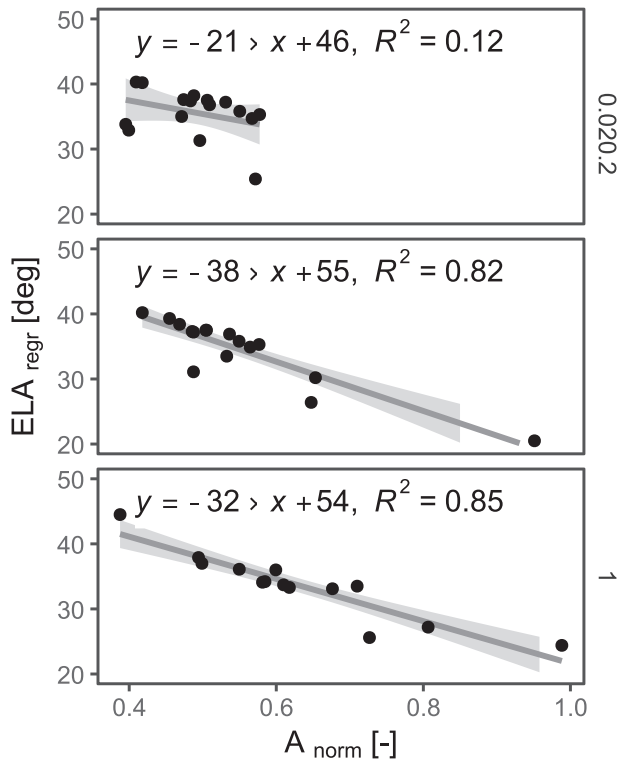


**Fig. 10.** Relationship between the retro-calculated ELA (ELA<sub>regr</sub>) and the normalized area below the transects (A<sub>norm</sub>), grouped by RVC.

The number of deposited blocks varied between the different transects and RVC (Table 3). The distribution of the deposited blocks along the transect was left-skewed for the two smaller RVC and rather irregular for RVC 1.0 (Fig. 5). The blocks of all transects were predominantly rectangular and consisting of limestone, except for transect number 16 where they were gneiss.

For all transects, a density of 2700 kgm<sup>-3</sup> was defined.

## 4. Methods

### 4.1. Retro-calculation of the energy line angle and initial rockfall height

RFN expresses the protective capacity of a forest as the percentage of stopped blocks at a specific point along a trajectory. By inverting the approach used by the RFN tool, we can deduce the ELA from the percentage of stopped blocks per volume class mapped in the field.

In a first step, we calculated the cumulative frequency (in %) of deposited blocks per RVC and sector *i* for each transect (Fig. 6). To do so, we summed all blocks of a given RVC between the starting point of the transect and a given sector of interest ( $n_{RVC,i}$ ) divided by the total number of mapped blocks belonging to the given RVC ( $N_{tot,RVC}$ ).

Subsequently, we calculated the basal area of the trees theoretically encountered by a block of a specific RVC between the foot of the rock face and its deposition sector *i* using standardised representative diameters ( $d_{RVC}$ ; 0.27, 0.59 or 1.0 m) for the three defined RVCs ( $BA_{RVC,i}$  in m<sup>2</sup>) following

$$BA_{RVC,i} = BA_i \cdot l_i \cdot d_{RVC} \quad (3)$$

where  $BA_i$  is the mean basal area of the forest (in m<sup>2</sup>·ha<sup>-1</sup>) and  $l_i$  is the horizontal length of the forested slope (in m) between the rock face and the deposition sector *i*.

In a next step, we calculated the energy head (*H*) of each RVC per sector *i*. The latter corresponds to the potential energy of a block representing one of the three RVC for the situation without forest. It was determined as the total energy to be dissipated by the forest to stop 100 % of the blocks until sector *i*. Therefore, we first calculated the basal area theoretically required to stop all blocks up to sector *i* ( $BA_{theor,i}$ ). This can be done by multiplying  $BA_{RVC,i}$  by the inverse cumulative frequency.

$$BA_{theor,i} = BA_{RVC,i} \cdot \frac{N_{tot,RVC}}{n_{RVC,i}} \quad (4)$$

The theoretical energy dissipation ( $\delta E_{theor,i}$ ) until sector *i* for a given RVC can then be calculated as follows:

$$\delta E_{theor,i} = BA_{theor,i} \cdot FE \cdot \delta E_{Abies} \quad (5)$$

$\delta E_{Abies}$  corresponds to the maximum energy (in J) that *Abies alba* (European silver fir) can dissipate per m<sup>2</sup> basal area ( $E^{Abies} = 568$  kJ·m<sup>-2</sup>; Dorren and Berger (2006)). *Abies alba* is used here since it was the reference species in the study of Dorren and Berger (2006), due to the fact that it was impacted most often during their rockfall

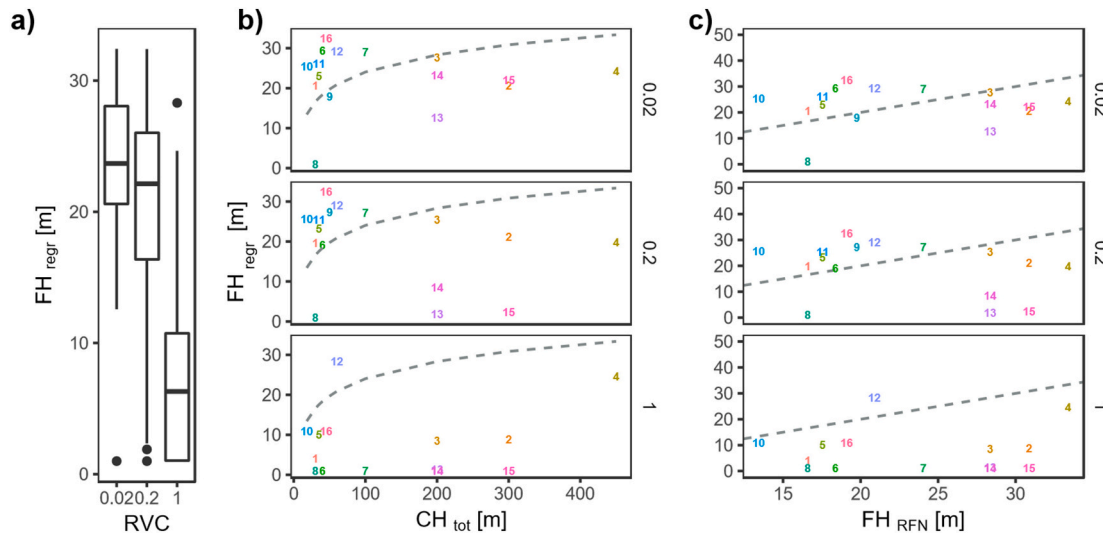


**Fig. 11.** FH resulting from the energy line based on the linear regression (FH<sub>regr</sub>). (a) Distribution of the retro-calculated initial fall heights (FH<sub>regr</sub>) per RVC; (b) Comparison of FH<sub>regr</sub> and the observed total rock face height (CH<sub>tot</sub>). The digits indicate the transect number whereas the dashed line represents the initial fall heights used by RFN<sub>2015</sub> as a logarithm of CH<sub>tot</sub>; (c) Comparison of FH<sub>regr</sub> and the initial fall heights of RFN<sub>2015</sub> (FH<sub>RFN</sub>). The digits indicate the transect number. FH<sub>regr</sub> is by default 1 m. The dashed line represents the 1:1 line.

experiments. It is multiplied by the weighted tree energy dissipation factor  $F_E$  of coniferous and deciduous trees along the transect (Eq. 6).

$$F_E = 0.9 \cdot P_{conif} + 1.1 \cdot (1 - P_{conif}) \quad (6)$$

where  $P_{conif}$  is the proportion of coniferous trees in the transect. It is multiplied with a species type specific energy dissipation factor (0.9 for conifers and 1.1 for deciduous trees), which represents the average energy reduction capacity of the species type relative to *Abies alba* (based on Moos et al., 2019).

Since the energy line method is quite conservative and occasionally produces high kinetic energies, the corresponding translational velocities can be unrealistically high, especially for small rock volumes. To ensure that RFN calculates realistic kinetic energy values for the given rock volume, the following transect-specific and slope-dependent velocity limit  $v_{lim}$  was defined by (Berger and Dorren, 2007):

$$v_{lim} = 0.64 \cdot \theta_T \quad (7)$$

where  $\theta_T$  is the mean slope angle of the transect (in °) (Fig. 1).

To check if  $\delta E_{theor,i}$  was realistic, we calculated the corresponding velocity ( $v_{RVC,i}$ ) based on the mass of a given RVC. The  $\delta H$  of a given RVC in sector  $i$  can finally be determined as:

$$\delta H_{RVC,i} = \begin{cases} \delta E_{theor,i} & \text{if } v_{RVC,i} \leq v_{lim} \\ \frac{(v_{lim,i})^2}{2g} & \text{otherwise} \end{cases} \quad (8)$$

Subsequently, we used a linear regression between the distance of the end of each sector  $i$  to the transect starting point and  $\delta H_{RVC,i}$  to determine the energy line per transect. This allows us to determine the energy line angle ( $ELA_{regr}$ ) and the initial fall height  $FH_{regr}$  corresponding to the intercept (Fig. 7).

#### 4.2. Evaluation of RFN performance using retro-calculated energy line angle and initial rockfall height

To evaluate the performance of RFN, we ran the tool for four different combinations of ELAs and FHs:

1. with the parameters as described in Dorren et al. (2015) (RFN<sub>2015</sub>),

2. with the transect- and RVC-specific ELA but with the fall height as calculated in RFN<sub>2015</sub> (see Eq. (2)) ( $ELA_{regr} + FH_{RFN}$ ),
3. with the constant ELA of 31° as used in RFN<sub>2015</sub>, but with the transect and RVC-specific FHs ( $ELA_{RFN} + FH_{regr}$ ) and
4. with the transect- and RVC-specific ELAs and their corresponding FHs (RFN<sub>regr</sub>).

If the  $FH_{regr}$  of a transect was negative due to a very low intercept resulting from the linear regression, a default value of 1 m was used in the calculation with RFN. We compared the resulting protective capacities (in terms of stopped blocks) with the cumulative percentage of stopped blocks mapped in each sector along the transect, which we considered as ground truth. The difference between both protective capacities was considered as error and used to calculate the root mean square error (RMSE) for the different RFN variants.

#### 4.3. Comparison of the retro-calculated ELA with the normalized area below the transect

Quarteroni (2017) analysed the relationship between various topographical indices and the ELAs of around 600 well-documented historical rockfall events throughout the European Alps. They found that these ELAs can be well described by an exponential function of the normalized area ( $A_{norm}$ ) below the trajectories of the mapped blocks.  $A_{norm}$  is based on the study of (Demoulin, 1998) and represents the total area of the slope profile under the rockfall trajectory, normalized by the total fall height of the block, both horizontally and vertically (for a graphical explanation see Fig. 8). In this study, we calculated  $A_{norm}$  as the sum of the normalized areas below each inventory sector  $i$  for the number of sectors  $n$  (Eq. (9)) and normalized both the horizontal ( $x_i$ ) and the vertical distance ( $z_i$ ) with  $z_n$  following (Quarteroni, 2017).

$$A_{norm} = \frac{1}{z_n^2} \sum_{i=0}^n ((z_i - z_{i-1}) \cdot x_{i-1}) + \frac{(z_i - z_{i-1}) \cdot (x_i - x_{i-1})}{2} \quad (9)$$

To evaluate whether the methodology of Quarteroni (2017) could provide a potential solution for the definition of a slope morphology dependent ELA, we compared  $A_{norm}$  for each transect to the  $ELA_{regr}$  and tested if a relationship exists between the two.

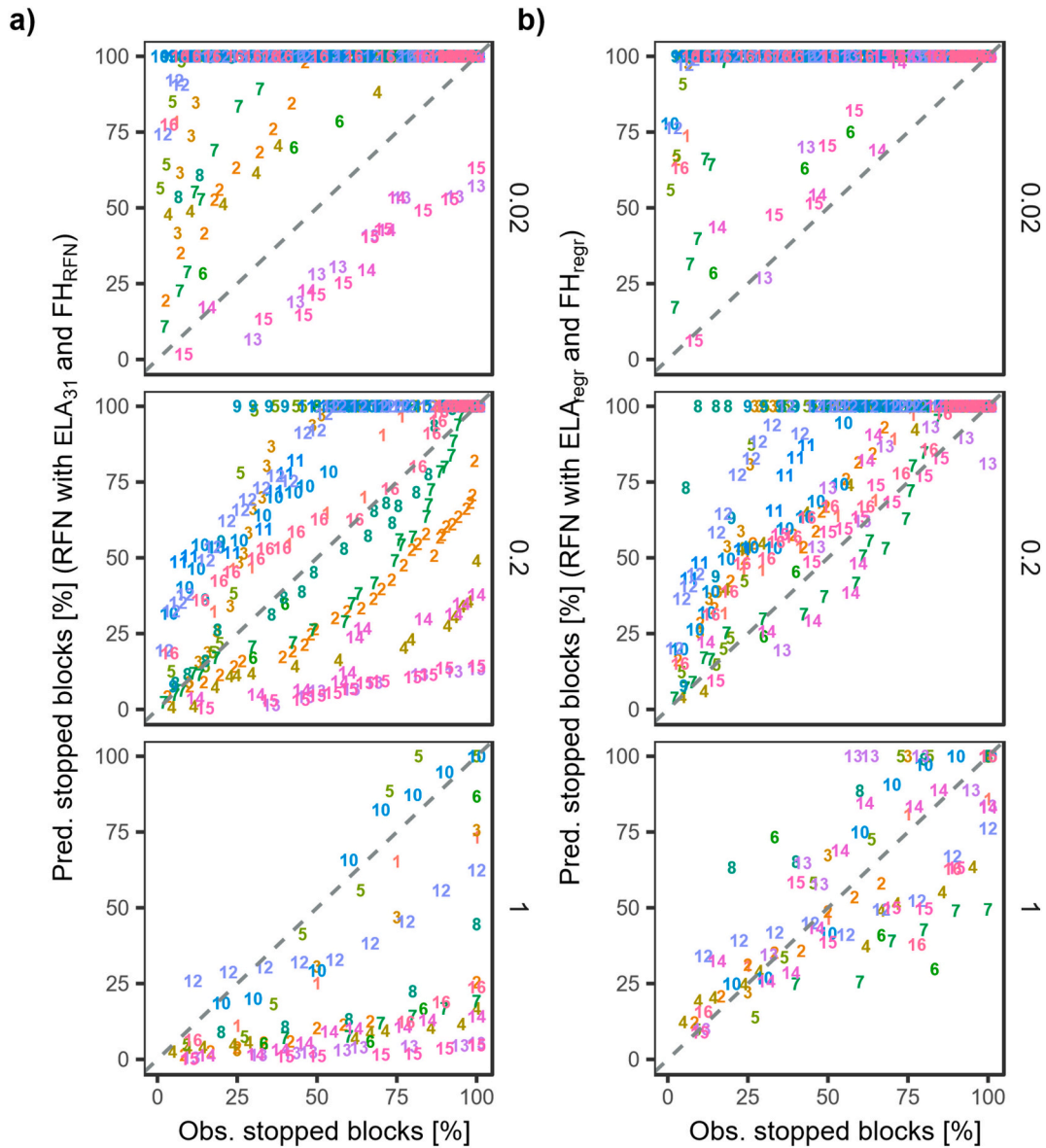


**Fig. 12.** Protection capacity of the forest in terms of stopped blocks at each transect sector and per RVC predicted with RFN versus observed. A point represents a specific sector and the number the corresponding transect.  
 (a) RFN used with a constant ELA of 31° and  $FH_{RFN}$ .  
 (b) RFN used with the transect- and RVC-specific ELA and FH.

**5. Results**

*5.1. Transect- and rock volume-specific energy line angles and initial fall heights*

The ELAs obtained with the inverted RFN approach are not constant but vary across all transects and RVC between 26.4° and 40.3° (adjusted for outliers; see Table 4 and Fig. 9 as well as detailed illustrations of single transects in Appendix A.14). The minimum  $R^2$  of the regressions used to determine the variable ELA was 0.96, the standard error varied between 0.001 m and 0.063 m (Appendix A.5). For transect 9 and 11 the specific ELA of RVC 1.0 could not be determined due to insufficient data points (i.e., sufficient deposited blocks in multiple sectors) for the linear regression.

The recalculated ELAs were on average larger than the fixed 31° used by RFN<sub>2015</sub>. The ELAs of RVC 1.0 are generally lower (median = 33.9°) compared to those of RVC 0.02 and 0.2 (median = 36.3°) (Fig. 9 and Table 4).  $ELA_{reg}$  is strongly negatively correlated with the normalized

area for RVC 1.0 ( $R^2 = 0.85$ ) and RVC 0.2 ( $R^2 = 0.82$ ), whereas for RVC 0.02 only a weak relationship can be observed ( $R^2 = 0.12$ ) (Fig. 10).

The FH obtained with the inverted RFN approach ( $FH_{reg}$ ) vary across all transects and RVC between 1 m and 32 m (Fig. 11 and Appendix A.5), generally decreasing with increasing RVC.

The  $FH_{reg}$  are generally lower compared to the observed rock face height ( $CH_{tot}$ ). There does not seem to be any relationship between  $FH_{reg}$  and  $CH_{tot}$  or  $FH_{RFN}$ , respectively (Fig. 11).

*5.2. RFN performance with retro-calculated energy line angles and fall heights*

The current version of RFN (RFN<sub>2015</sub>) mostly overestimated the protective function of forests for RVC 0.02 except for transects 13, 14 and 15 (Fig. 12) with a median root mean squared error (RMSE) of 34.2 % (Fig. 13). For RVC 0.2, the predictions of RFN<sub>2015</sub> show a large variability but with a lower median RMSE compared to RVC 0.02 (28.5 %). For RVC 1.0, RFN<sub>2015</sub> clearly underestimated the protective function

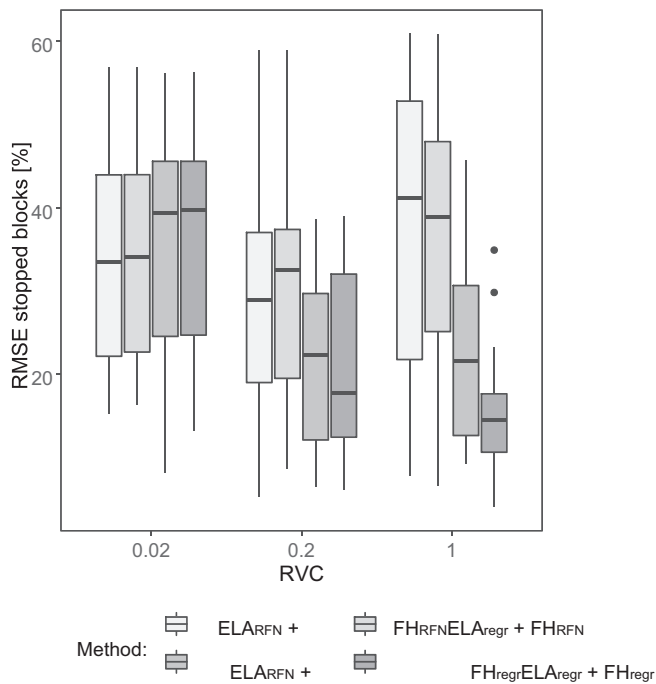


Fig. 13. Root mean squared error (RMSE) of predicted number of stopped rock per RVC and method.

of forests (except for transects 5 and 10) with a median RMSE of 37.4 %. With trajectory-specific ELAs, but FH as used in RFN, the RMSE could only be slightly reduced or was even increased (Fig. 13). Using  $FH_{regr}$  instead of  $FH_{RFN}$  remarkably reduced the errors for RVC 1.0 and RVC 0.2. In contrast, the errors of RVC 0.02 increased compared to  $RFN_{2015}$ . For some transects of RVC 1.0, the  $FH_{regr}$  had to be set by default to 1 m because the intercept of the linear regression led to negative FH. Finally, using RFN with both  $FH_{regr}$  and  $ELA_{regr}$  yielded minimum RMSE for RVC 0.2 and 1.0, but largest RMSE for RVC 0.02.

6. Discussion

Based on the approach used in this study, we could reconstruct the energy lines of observed deposited blocks for 16 different rockfall slopes in Switzerland. The linear regression of the recalculated energy heads provided energy line angles (ELA) specific for the transect and rock volume classes (RVC) and representative initial fall heights (FH) per transect. The results clearly showed that there is a large variability in transect-specific ELA with values considerably different from a fixed ELA of 31°. Using RFN with these transect- and RVC-specific ELAs and FHs (hereafter referred to as  $RFN_{best}$ ) leads to a remarkably better estimate of the protective capacity of a forest in comparison to  $RFN_{2015}$ , especially for RVC 1.0 (reduction of the mean RMSE from 41.1 % to 14.5 %) and to a lesser extent for RVC 0.2. For the smallest RVC, the prediction of the protective capacity could not be improved. The improvement was mainly due to the use of trajectory-specific FHs, while using only the trajectory-specific ELAs did not lead to better predictions. This can be explained by the fact that a slight change in the ELA influences the extreme block deposition points only marginally compared to a shift of the energy line by increasing or decreasing the FH.

All tested variants of RFN clearly overestimated the protective capacity of the forest for the smallest RVC. The reason why none of them was capable to reproduce the deposition pattern of RVC 0.02 adequately is probably that they mostly originated from fragmentation of larger blocks during down-slope propagation. This leads to small blocks (which are in fact fragments) that are deposited relatively far from the source area. As a consequence, we found unexpectedly small ELAs for the

smallest RVC for certain transects.

It is striking that the rock deposition patterns at transects 13, 14 and 15 of RVC 0.2 and 0.02 are all badly represented by  $RFN_{2015}$ . On these transects, 30 % of the rock fragments are deposited close to the rock face (within the first 20 to 40 m; Appendix A.14). These transects are close to older rock slide deposits which destroyed parts of the forest and, thus, we assume that the dominant process on these transects is rock sliding. Typical for this process is that a large portion of the fallen mass is deposited in the upper part of the transit area and only large blocks and boulders propagate down the transit slope. Hence the observed deposition pattern could be explained by the direct fragmentation and interaction between blocks rather than by the effect of the forest. In the end, we assumed that all transect were comparable regarding slop surface roughness. When comparing the slope transects overall, this might be true, but not for individual sectors. In other words, when looking at, for example, the first two sectors in all transects, one would see that these do not have exactly the same surface conditions, which surely also explains differences in the deposition patterns. However, if we start taking the number of fresh deposited blocks, which do form a given roughness on the slope, into account as a factor of energy loss, we end up in a chicken or the egg causality dilemma. In the case we could not have calculated the energy heads based on the forest characteristics, which forms the basis of this study. Therefore, the assumption that the slope surface roughness could be neglected was required.

The initial fall heights based on the linear regressions ( $FH_{regr}$ ) are all substantially smaller than the observed rock face heights ( $CH_{tot}$ ) and in the same range as those used by  $RFN_{2015}$ . This confirms the basic assumption in  $RFN_{2015}$ , which considers the initial FH as a representation of the last vertical drop of a falling block after the last rebound in the rock face. However, the logarithmic function used by  $RFN_{2015}$  to calculate the initial fall height based on  $CH_{tot}$  did not produce realistic results when compared to  $FH_{regr}$ . Additional analyses of  $FH_{regr}$  in relationship to the slope angle, the basal area or the total rock face height, did not reveal any logical explanations. Therefore, finding a robust method that determines the representative energetic initial fall height remains a major challenge. The  $FH_{regr}$  is determined by the energy heads of the deposited blocks, which is mainly determined by the basal area encountered by a block until its deposition sector and the mean slope angle. In almost all transects, the energy head of RVC 0.02 and 0.2 was limited by a threshold based on the mean slope angle since the blocks exceeded the maximum allowed velocity (Appendix B.15). The fact that mainly these RVCs are concerned by that velocity limit can be explained by the EL-based calculated energies which are too high in comparison to the relatively small block masses.

The comparison of the retro-calculated energy line angle with the normalized area below the normalized area revealed a strong relationship between the two, especially for RVC 0.2 and 1.0. Hence the normalized area method proposed by Quarteroni (2017) is a promising alternative for estimating accurate trajectory specific ELA. What is needed is a detailed analysis on an exhaustive database with rockfall events that includes a range of forest situations, rock volumes and slope surface types for a large variety of topographies.

7. Conclusions

By reconstructing the energy line angles of deposited blocks we could evidence that they highly depend on the volumes and the trajectories of the fallen blocks. Therefore, a solution has to be found for integrating a topography-based ELA in RFN instead of using a constant ELA of 31°. Similarly, the reconstructed fall heights were significantly smaller than the observed rock face heights. Using these transect and block volume specific ELAs and FHs could remarkably improve the predictions of the protective capacity of forests by the  $RockFor^{NET}$  tool for blocks with a volume between 0.2 and 1.0. However, our results did not allow for the development of a method for estimating representative energetic fall heights on the basis of the total observed rock face height. Furthermore,

the normalized area approach described by Quarteroni (2017) provided promising results in deriving trajectory-specific ELAs. The analysis of additional inventory data of rockfall deposits from a large variety of sites is required to derive a robust and reliable method for predicting the ELA of a given rockfall trajectory.

**Declaration of competing interest**

The authors declare the following financial interests/personal relationships which may be considered as potential competing interests:

Luuk Dorren reports financial support was provided by European Union - Interreg Alpine Space. Julia Menk reports financial support was provided by European Union - Interreg Alpine Space. Frederic Berger

reports financial support was provided by European Union - Interreg Alpine Space.

**Data availability**

Data will be made available on request.

**Acknowledgements**

We thank Walter Krättli, Serge Borer, Marco von Glutz, Grégory Amos, Jean-Jacques Thormann, Kaspar Zürcher and Yves Wiedmer for their contribution to this study. We further acknowledge the EU Interreg Alpine Space Programme for funding the RockTheAlps project.

**Appendix A. Transect and rock volume specific energy line angles and fall heights**

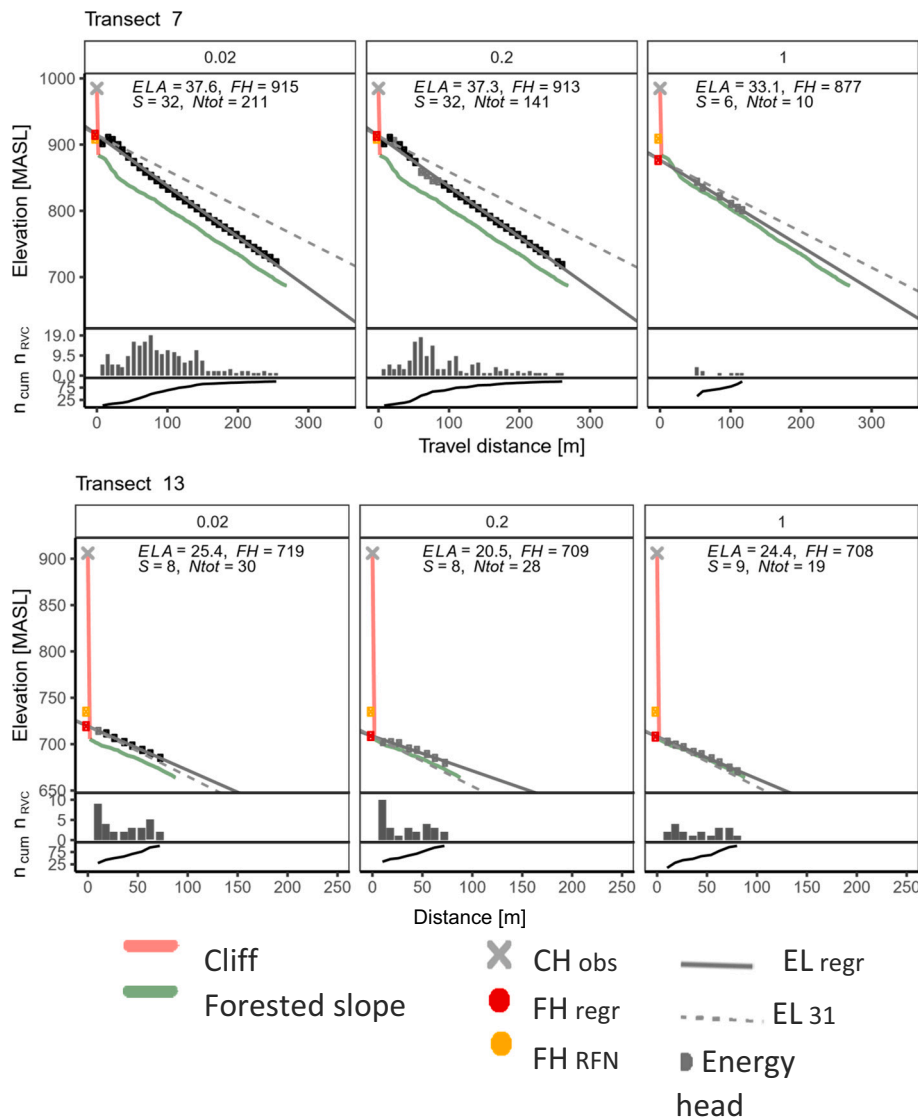


**Fig. A.14.** Profiles of transects numbers 7 and 13 per rock volume class (RVC). ELA: energy line angle; S: number of sectors per transect; Ntot: total number of observed blocks per RVC; CH<sub>obs</sub>: total rock face height observed in the field; FH<sub>regr</sub>: intercept of the energy heads representing the fall height of that specific RVC and transect. FH<sub>RFN</sub>: FH determined by RFN<sub>2015</sub>; EL<sub>regr</sub>: energy line resulting from linear regression of the energy heads; EL31: energy line of 31°; n<sub>RVC</sub>: number of deposited blocks per transect sector and RVC; n<sub>cum</sub>: cumulative number of deposited blocks in %.

**Table A.5**

Transect (T) and rock volume class (RVC) specific energy line angles (ELA) and fall heights (FH) derived with the inverted RFN-approach using a linear regression between the reconstructed energy heads of a falling block. Corr: correlation coefficient between  $ELA_{reg}$  and  $FH_{reg}$ ; SE: standard error of the linear regression;  $\Delta_{FH-CH}$ : difference between the  $FH_{reg}$  and the observed rock face height. RMSE: root mean squared errors of the prediction of the protective capacity of the forest (in terms of stopped blocks). Missing values (–) indicate insufficient data for linear regression.

T	RVC	$ELA_{reg}$	$FH_{reg}$	Corr	SE	$\Delta_{FH-CH}$	RMSE $RFN_{reg}$	RMSE $RFN_{2015}$
	[m <sup>3</sup> ]	[°]	[m]		[m]	[m]	[%]	[%]
1	0.2	31.1	20	–0.99	0.02	–10	12.5	13.0
1	1	25.6	4	–0.99	0.03	–26	7.4	18.8
2	0.02	34.7	21	–0.99	0.01	–279	33.2	22.3
2	0.2	34.9	21	–0.99	0.01	–279	15.3	23.1
2	1	34.2	9	–0.99	0.02	–291	4.1	35.7
3	0.02	38.2	28	–0.99	0.01	–172	45.5	40.8
3	0.2	37.5	25	–0.99	0.01	–175	35.7	23.7
3	1	34.1	9	–0.99	0.02	–191	11.3	23.5
4	0.02	35.0	24	–1.000	0.00	–426	42.3	21.2
4	0.2	33.5	20	–0.99	0.02	–430	13.9	36.8
4	1	37.0	25	–0.99	0.04	–425	13.6	43.4
5	0.02	35.3	23	–1.00	0.00	–12	41.1	40.8
5	0.2	35.3	23	–1.00	0.00	–12	29.8	29.1
5	1	33.3	10	–1.00	0.01	–25	10.5	11.0
6	0.02	40.3	29	–1.00	0.02	–11	13.3	15.3
6	0.2	39.3	19	–1.00	0.01	–21	20.2	21.0
6	1	36.1	1	–0.99	0.06	–39	29.8	42.2
7	0.02	37.6	29	–1.00	0.01	–71	25.2	21.9
7	0.2	37.3	27	–0.99	0.01	–73	6.7	11.1
7	1	33.1	1	–1.00	0.02	–99	34.9	60.5
8	0.02	37.4	1	–1.00	0.01	–29	38.3	34.4
8	0.2	37.2	1	–1.00	0.01	–29	38.3	5.3
8	1	36.0	1	–1.00	0.03	–29	23.2	40.0
9	0.02	36.8	18	–1.00	0.01	–32	52.0	52.0
9	0.2	38.4	27	–1.00	0.02	–23	38.9	37.8
9	1	–	–	–	–	–	–	–
10	0.02	35.8	25	–1.00	0.01	7	56.3	56.9
10	0.2	35.8	26	–1.00	0.01	8	24.9	28.8
10	1	33.7	11	–1.00	0.01	–7	9.9	7.8
11	0.02	37.2	26	–1.00	0.01	–9	45.7	45.7
11	0.2	36.9	25	–1.00	0.01	–10	30.8	30.0
11	1	–	–	–	–	–	–	–
12	0.02	37.5	29	–1.00	0.00	–31	46.7	46.1
12	0.2	37.5	29	–1.00	0.00	–31	35.7	29.8
12	1	37.9	28	–1.00	0.02	–32	16.9	21.2
13	0.02	25.4	13	–1.00	0.01	–187	23.3	28.4
13	0.2	20.5	2	–0.98	0.03	–198	12.5	58.9
13	1	24.4	1	–0.99	0.01	–199	17.7	55.4
14	0.02	32.9	23	–1.00	0.01	–177	13.6	16.4
14	0.2	26.4	8	–0.98	0.04	–192	12.4	43.8
14	1	27.2	1	–0.99	0.02	–199	11.1	48.8
15	0.02	33.8	22	–0.99	0.02	–278	15.4	28.3
15	0.2	30.2	2	–0.99	0.01	–298	6.2	54.9
15	1	33.5	1	–1.00	0.02	–299	15.4	60.9
16	0.02	40.2	32	–1.00	0.01	–13	32.1	32.7
16	0.2	40.2	32	–1.00	0.01	–13	10.7	9.5
16	1	44.5	11	–0.98	0.14	–34	17.6	54.1

Appendix B. Sectors with slope-based velocity limitation

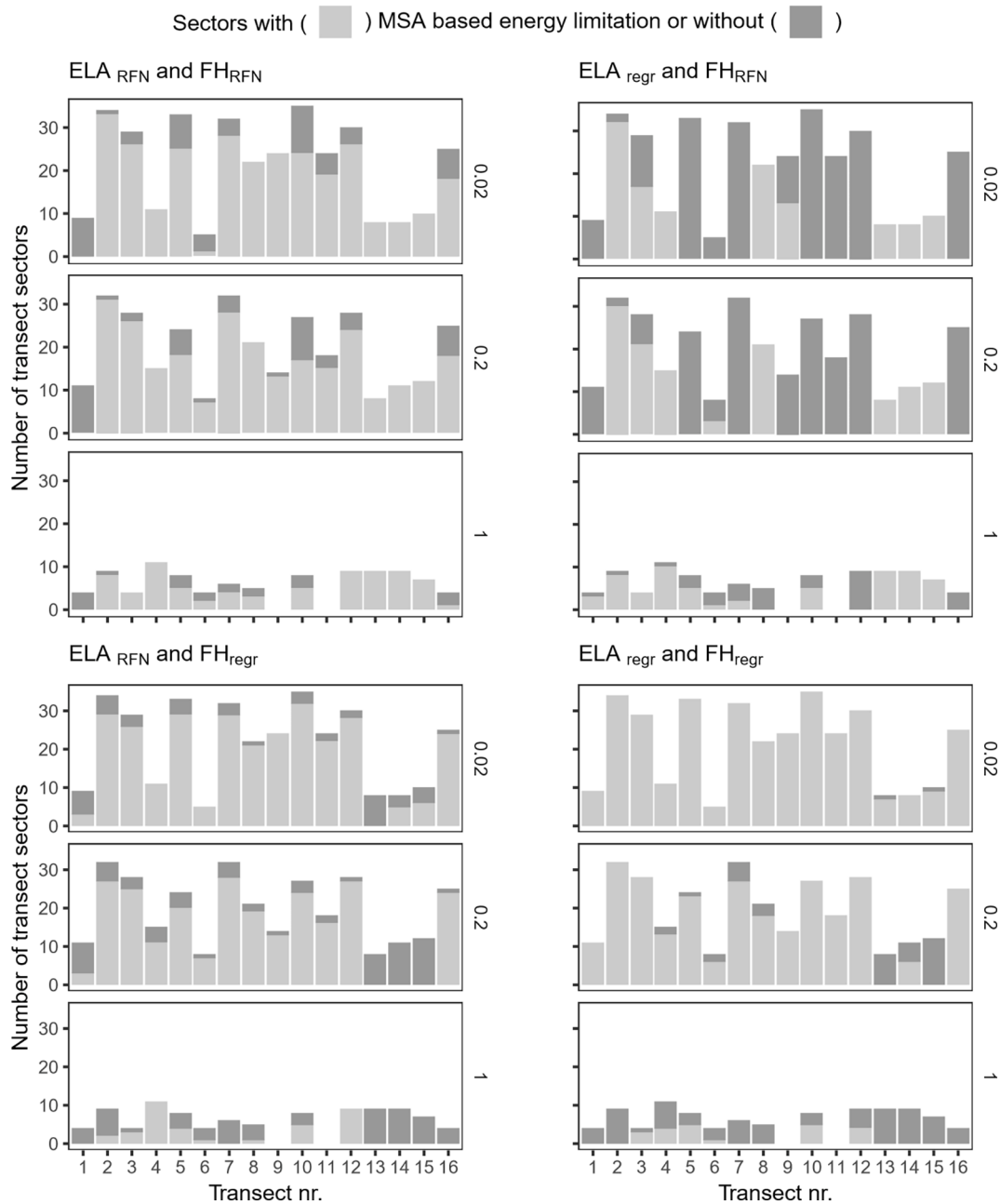


Fig. B.15. Number of sectors per transect where the blocks exceeded the defined maximum velocity, which required limitation by the slope-based threshold. MSA: mean slope angle.

References

Berger, F., Dorren, L.K., 2007. Principles of the tool rockfor.net for quantifying the rockfall hazard below a protection forest. *Schweiz. Z. Forstwes.* 158, 157–165. <https://doi.org/10.3188/szf.2007.0157>.

Borella, J., Quigley, M., Krauss, Z., Lincoln, K., Attanayake, J., Stamp, L., Lanman, H., Levine, S., Hampton, S., Gravley, D., 2019. Geologic and geomorphic controls on rockfall hazard: how well do past rockfalls predict future distributions? *Nat. Hazards Earth Syst. Sci.* 19, 2249–2280. <https://doi.org/10.5194/nhess-19-2249-2019>.

Borgniet, L., Toe, D., Berger, F., Galvagno, M., Panigada, C., Colombo, R., Di Cella, U.M., Gottardelli, S., Rollet, I., Negro, M., Vertui, F., Fermont, C., 2013. Monitoring climatic change impacts on protection forests in aosta valley (Italy) and in drôme (France) using medium and high resolution remote sensing and mateloscopes plots. In: Cerbu, G. (Ed.), *Management Strategies to Adapt Alpine Space Forests to Climate Change Risks*. InTech. <https://doi.org/10.5772/56281>.

Bourrier, F., Berger, F., Tardif, P., Dorren, L., Hungri, O., 2012. Rockfall rebound: comparison of detailed field experiments and alternative modelling approaches. *Earth Surf. Process. Landf.* 37, 656–665.

Caviezel, A., Gerber, W., 2018. Brief communication: measuring rock decelerations and rotation changes during short-duration ground impacts. *Nat. Hazards Earth Syst. Sci.* 18, 3145–3151. <https://doi.org/10.5194/nhess18-3145-2018>.

Corominas, J., Copons, R., Vilaplana, J.M., Altimir, J., Amigó, J., 2003. Integrated landslide susceptibility analysis and hazard assessment in the principality of andorra. *Nat. Hazards* 30, 421–435. <https://doi.org/10.1023/B:NHAZ.000007094.74878.d3>.

Demoulin, A., 1998. Testing the tectonic significance of some parameters of longitudinal river profiles: the case of the Ardenne (Belgium, NW Europe). *Geomorphology* 24, 189–208. [https://doi.org/10.1016/S0169-555X\(98\)00016-6](https://doi.org/10.1016/S0169-555X(98)00016-6).

Dorren, L., 2016. *Rockyfor3d (v5.2) revealed: transparent description of the complete 3d rockfall model*. <https://www.ecorisq.org/docs/Rockyfor3Dv52EN.pdf>.

- Dorren, L., Berger, F., Frehner, M., Huber, M., Kühne, K., Métral, R., Sandri, A., Schwitler, R., Thormann, J.J., Wasser, B., 2015. Das neue Nais-Anforderungsprofil Steinschlag. *Schweizerische Zeitschrift für Forstwesen* 166, 16–23.
- Dorren, L., Berger, F., Jonsson, M., Krautblatter, M., Mölk, M., Stoffel, M., Wehrli, A., 2007. State of the art in rockfall – forest interactions. *Schweiz. Z. Forstwes.* 158, 128–141. <https://doi.org/10.3188/szf.2007.0128>.
- Dorren, L., Berger, F., Le Hir, C., Mermin, E., Tardif, P., 2005. Mechanisms, effects and management implications of rockfall in forests. *For. Ecol. Manag.* 215, 183–195. <https://doi.org/10.1016/j.foreco.2005.05.012>.
- Dorren, L., Maier, B., Putters, U.S., Seijmonsbergen, A.C., 2004. Combining field and modelling techniques to assess rockfall dynamics on a protection forest hillslope in the European alps. *Geomorphology* 57, 151–167. [https://doi.org/10.1016/S0169-555X\(03\)00100-4](https://doi.org/10.1016/S0169-555X(03)00100-4).
- Dorren, L., Wehrli, A., 2013. Protection forests: a key factor in integrated risk management in the alps. In: Renaud, F.G., Sudmeier-Rieux, K., Estrella, M. (Eds.), *The Role of Ecosystems in Disaster Risk Reduction*. United Nations University Press, Shibuya-ku, Tokyo, pp. 321–342.
- Dorren, L.K.A., Berger, F., 2006. Stem breakage of trees and energy dissipation during rockfall impacts. *Tree Physiol.* 26, 63–71. <https://doi.org/10.1093/treephys/26.1.63>.
- Erisman, T.H., Abele, G., 2001. *Dynamics of Rockslides and Rockfalls: With 10 Tables*. Springer, Berlin.
- Frehner, M., Wasser, B., Schwitler, R., 2005. Nachhaltigkeit und Erfolgskontrolle im Schutzwald: Wegleitung für Pflegemaßnahmen in Wäldern mit Schutzfunktion: Vollzug Umwelt. Bundesamt für Umwelt, Wald und Landschaft (BUWAL), Bern.
- Frehner, M., Wasser, B., Schwitler, R., 2007. Sustainability and Success Monitoring in Protection Forests: Guidelines for Silvicultural Interventions in Forests With Protective Functions. Volume 27/07 of Environmental Studies. Federal Office for the Environment (FOEN), Bern.
- Hantz, D., Corominas, J., Crosta, G.B., Jaboyedoff, M., 2021. Definitions and concepts for quantitative rockfall hazard and risk analysis. *Geosciences* 11, 158.
- Heim, A., 1932. *Bergsturz und Menschenleben*. Fretz & Wasmuth, Zürich.
- Heinimann, H.R., Hollenstein, K., Kienholz, H., Krummenacher, B., Mani, P., 1998. Methoden zur Analyse und Bewertung von Naturgefahren: eine risikoorientierte Betrachtungsweise. volume 85 of *Umwelt-Materialien Naturgefahren*. Schweiz Bundesamt für Umwelt, Wald und Landschaft BUWAL, Bern.
- Hsü, K.J., 1975. Catastrophic debris streams (sturzstroms) generated by rockfalls. *Geol. Soc. Am. Bull.* 86, 129. [https://doi.org/10.1130/00167606\(1975\)86<129:CDSSGB>2.0.CO;2](https://doi.org/10.1130/00167606(1975)86<129:CDSSGB>2.0.CO;2).
- Jaboyedoff, M., Labiouse, V., 2003. Preliminary assessment of rockfall hazard based on gis data. In: 10th International Congress on Rock Mechanics. International Society for Rock Mechanics and Rock Engineering, pp. 575–578.
- Jaboyedoff, M., Labiouse, V., 2011. Technical note: preliminary estimation of rockfall runout zones. *Nat. Hazards Earth Syst. Sci.* 11, 819–828. <https://doi.org/10.5194/nhess-11-819-2011>.
- Lanfranconi, C., Sala, G., Frattini, P., Crosta, G., Valagussa, A., 2020. Assessing the rockfall protection efficiency of forests at the regional scale. *Landslides* 17, 2703–2721.
- Lu, G., Ringenbach, A., Caviezel, A., Sanchez, M., Christen, M., Bartelt, P., 2021. Mitigation effects of trees on rockfall hazards: does rock shape matter? *Landslides* 18, 59–77.
- Maringer, J., Ascoli, D., Dorren, L., Bebi, P., Conedera, M., 2016. Temporal trends in the protective capacity of burnt beech forests (*Fagus sylvatica* L.) against rockfall. *Eur. J. For. Res.* 135, 657–673. <https://doi.org/10.1007/s10342-016-0962-y>.
- Meissl, G., 1998. Modellierung der Reichweite von Felsstürzen: Fallbeispiele zur GIS-gestützten Gefahrenbeurteilung aus dem Bayerischen und Tiroler Alpenraum; mit 24 Tabellen. Selbstverl. d. Inst. für Geographie d. Univ.
- Moos, C., Dorren, L., Stoffel, M., 2017. Quantifying the effect of forests on frequency and intensity of rockfalls. *Nat. Hazards Earth Syst. Sci.* 17, 291–304. <https://doi.org/10.5194/nhess-17-291-2017>.
- Moos, C., Toe, D., Bourrier, F., Knüsel, S., Stoffel, M., Dorren, L., 2019. Assessing the effect of invasive tree species on rockfall risk—the case of *Ailanthus altissima*. *Ecol. Eng.* 131, 63–72.
- Onofri, R., Candian, C., 1979. Indagine sui limiti di massima invasione dei blocchi franati dovuti al sisma del Friuli del 1976. considerazione delle opere di difesa. In: *Reg. Aut. Friuli Venezia Giulia-Univ. di Trieste. Ist. Geol. e Paleont. Trieste*, p. 42.
- Quarteroni, A., 2017. Modélisation statistique pour l'aide à la cartographie de l'aléa chutes de blocs: Influence de la topographie du versant et du couvert forestier. Mémoire de fin d'études dominante d'approfondissement gestion forestière. AgroParisTech, Saint-Martin-d'Hères, France.
- Saroglou, H., Berger, F., Bourrier, F., Asteriou, P., Tsiambaos, G., Tsagkas, D., 2015. Effect of forest presence on rockfall trajectory. An example from Greece. In: *Engineering Geology for Society and Territory-Volume 2*. Springer, Cham, pp. 1899–1903.
- Scheidegger, A.E., 1973. On the prediction of the reach and velocity of catastrophic landslides. *Rock Mechanics* 5 (4), 231–236.
- Swisstopo, 2014. swissALTI3D. URL: Federal Office of Topography, Wabern, Switzerland. <https://www.swisstopo.admin.ch/en/geodata/height/alti3d.html>. (Accessed 1 November 2022).
- Toppe, R., 1987. Terrain models: A tool for natural hazard mapping. *IAHS Publication* 162, 629–638.
- Vick, L.M., Zimmer, V., White, C., Massey, C., Davies, T., 2019. Significance of substrate soil moisture content for rockfall hazard assessment. *Natural Hazards and Earth System Sciences* 19 (5), 1105–1117.
- Wehrli, A., Dorren, L., Berger, F., Zingg, A., Schönenberger, W., Brang, P., 2006. Modelling long-term effects of forest dynamics on the protective effect against rockfall. *Forest Snow and Landscape Research* 80, 57–76.
- Wieczorek, G.F., Morrissey, M.M., Iovine, G., Godt, J., 1999. Rock-fall potential in the Yosemite Valley, California. *US Geological Survey Open-File Report* 99 (578), 1–7.
- Wyllie, D.C., 2014. *Rock Fall Engineering*. CRC Press, Boca Raton FL, USA, p. 270.
- Žabota, B., Repe, B., Kopal, M., 2019. Influence of digital elevation model resolution on rockfall modelling. *Geomorphology* 328, 183–195.